Antifungal symbiotic peptide NCR044 exhibits unique structure and multifaceted mechanisms of action that confer plant protection

Siva L. S. Velivelli[a], Kirk J. Czymmek[a,b], Hui Li[a], Jared B. Shaw[c], Garry W. Buchko[c,d], and Dilip M. Shah[a,1]

[a]Donald Danforth Plant Science Center, St Louis, MO 63132; [b]Advanced Bioimaging Laboratory, Donald Danforth Plant Science Center, St Louis, MO 63132; [c]Earth and Biological Sciences Directorate, Pacific Northwest National Laboratory, Richland, WA 99354; and [d]School of Molecular Biosciences, Washington State University, Pullman, WA 99164

Edited by Maria J. Harrison, Cornell University, Ithaca, NY, and approved May 26, 2020 (received for review February 26, 2020)

In the indeterminate nodules of a model legume *Medicago truncatula*, ~700 nodule-specific cysteine-rich (NCR) peptides with conserved cysteine signature are expressed. NCR peptides are highly diverse in sequence, and some of these cationic peptides exhibit antimicrobial activity in vitro and in vivo. However, there is a lack of knowledge regarding their structural architecture, antifungal activity, and modes of action against plant fungal pathogens. Here, the three-dimensional NMR structure of the 36-amino acid NCR044 peptide was solved. This unique structure was largely disordered and highly dynamic with one four-residue α-helix and one three-residue antiparallel β-sheet stabilized by two disulfide bonds. NCR044 peptide also exhibited potent fungicidal activity against multiple plant fungal pathogens, including *Botrytis cinerea* and three *Fusarium* spp. It inhibited germination in quiescent spores of *B. cinerea*. In germlings, it breached the fungal plasma membrane and induced reactive oxygen species. It bound to multiple bioactive phosphoinositides in vitro. Time-lapse confocal and superresolution microscopy revealed strong fungal cell wall binding, penetration of the cell membrane at discrete foci, followed by gradual loss of turgor, subsequent accumulation in the cytoplasm, and elevated levels in nucleoli of germlings. Spray-applied NCR044 significantly reduced gray mold disease symptoms caused by the fungal pathogen *B. cinerea* in tomato and tobacco plants, and postharvest products. Our work illustrates the antifungal activity of a structurally unique NCR peptide against plant fungal pathogens and paves the way for future development of this class of peptides as a spray-on fungistat/fungicide.

NCR peptides | NMR structure | antifungal activity | gray mold disease | tomato

Medicago truncatula, a model legume of the inverted repeat-lacking clade (IRLC), forms an agriculturally important nitrogen-fixing endosymbiotic relationship with the gram-negative bacterium *Sinorhizobium meliloti* (1). This relationship results in the formation of indeterminate nodules on the roots of this plant, and its continued peaceful existence depends on the mutual exchange of signals between the host and its natural symbiotic bacterial partner. After endocytosis into the cytoplasm of specialized nitrogen-fixing nodule cells, microsymbiont *S. meliloti* undergoes a remarkable irreversible differentiation process leading to the formation of enlarged polyploid bacteroides. This terminal differentiation process is orchestrated by ~700 nodule-specific cysteine-rich (NCR) peptides expressed in successive spatiotemporal waves during nodule development (2–4). Genetic studies have revealed that the absence of specific NCR peptides results in the breakdown of the symbiotic relationship and the cessation of nitrogen fixation in *M. truncatula* (5–7).

NCR peptides are directed to the plant-derived symbiosome containing bacteroids via the plant secretory pathway. Thus, each peptide is synthesized as a larger precursor protein containing the amino-terminal endoplasmic reticulum-targeting signal and the mature bioactive peptide. NCR peptides are 30 to 50 amino acids in length but highly variable in their primary amino acid sequences and net charge. They are characterized by the presence of either four or six conserved cysteines presumably involved in formation of two or three intramolecular disulfide bonds. They are defensin-like since their predicted disulfide bonding patterns exhibit similarity with those of mammalian defensins. A subset of ~700 NCR peptides is cationic with a net charge ranging from +3 to +11 and is also rich in hydrophobic residues (8). Defensin-like NCR peptides exhibit potent antibacterial activity in vitro against symbiotic rhizobial bacteria and against various gram-negative and gram-positive bacteria (9–11). For example, NCR247 has antibacterial activity against free-living *S. meliloti* at high concentrations but induces bacteroid-like features at low concentrations. A mode-of-action (MOA) study showed that NCR247 blocks cell division, induces cell elongation, and forms complexes with bacterial ribosomal proteins affecting protein synthesis and the bacterial proteome (12). Since several hundred cationic NCR peptides are expressed in *M. truncatula*, it is likely that they exhibit different antibacterial MOA in different compartments of the nodule (13).

Significance

Several nodule-specific cysteine-rich (NCR) peptides expressed in a model legume *Medicago truncatula* exhibit potent antimicrobial activity. However, their structure–activity relationships and mechanisms of action against fungal pathogens of plants are still largely unknown. A small highly cationic peptide NCR044 with potent antifungal activity has been identified. This peptide has a unique highly dynamic structure and exhibits multifaceted mechanisms of action against a fungal pathogen *Botrytis cinerea*. Exogenous application of this peptide confers resistance to a gray mold disease caused by *B. cinerea* in tobacco and tomato plants as well as postharvest products. Our work paves the way for future development of NCR peptides as spray-on antifungal agents.

Author contributions: S.L.S.V., K.J.C., H.L., G.W.B., and D.M.S. designed research; S.L.S.V., H.L., J.B.S., and G.W.B. performed research; S.L.S.V., K.J.C., H.L., J.B.S., G.W.B., and D.M.S. analyzed data; S.L.S.V., K.J.C., H.L., G.W.B., and D.M.S. wrote the paper.

The authors declare no competing interest.

This article is a PNAS Direct Submission.

Data deposition: The coordinates of the NMR structure have been deposited in the Protein Data Bank, www.rcsb.org (PDB code: 6U6G) and the NMR chemical shifts have been deposited in the BioMagResBank, www.bmrb.wisc.edu (accession no. 30660).

[1]To whom correspondence may be addressed. Email: dshah@danforthcenter.org.

This article contains supporting information online at https://www.pnas.org/lookup/suppl/doi:10.1073/pnas.2003526117/-/DCSupplemental.

First published June 22, 2020.

In a recent study, 19 cationic NCR peptides were tested for their ability to inhibit the growth of a clinically relevant human fungal pathogen *Candida albicans*. Of these, nine with a net charge above +9 killed this fungal pathogen efficiently, showing fungicidal effects on both the yeast and hyphal forms at concentrations ranging from 1.5 to 10.5 μM, demonstrating their potential for development as antifungal drugs (8). The subcellular localization and intracellular targets of these peptides in fungal cells remain to be determined. There are several cationic NCR peptides with sequence heterogeneity expressed in the nodules of *M. truncatula* and other IRLC legumes, and it is likely that at least some of them have potent antifungal activity against plant fungal pathogens and are unique in structure and MOA.

In this study, we showed that NCR044, a 36-amino acid peptide with a net charge of +9 (8), exhibited potent antifungal activity against plant fungal pathogens. However, its three-dimensional (3D) NMR structure was determined to be very different from other well-characterized plant antifungal peptides such as defensins, thionins, lipid-transfer proteins, thaumatins, and heveins (14). This peptide localizes to the nucleolus in fungal cells, the site of ribosomal biogenesis. NCR044 conferred strong resistance to *B. cinerea* when applied topically on lettuce leaves and rose petals. Young tomato and *Nicotiana benthamiana* plants sprayed with this peptide were also protected from the gray mold disease caused by this pathogen, thus warranting further validation of the potential of NCR044 as a peptide-based fungistat/fungicide. Our work illustrates the antimicrobial activity of NCR peptides and paves the way for development of these peptides as a spray-on antifungal agent.

Results

Two NCR044 Homologs Are Expressed in the Nodules of *M. truncatula*. The *M. truncatula* genome contains genes encoding two NCR044 homologs, NCR044 (MtrunA17_Chr7g0216231) and NCR473 (MtrunA17_Chr7g0216241). The gene for each peptide encodes a signal sequence and a bioactive mature peptide. The mature peptides are each 36 amino acids in length and share 83% sequence identity (Fig. 1*A*). NCR044 has a net charge of +9 and 38% hydrophobic residues, whereas NCR473 has a net charge of +8 and 36% hydrophobic residues (Fig. 1*B*). Only two amino acid substitutions (I17P and R36S) account for the difference in net charge and hydrophobicity. The sequence of each mature peptide has a remarkably high concentration of cationic residues in the carboxyl-terminal half of each molecule. The primary sequence of each peptide displays no significant homology with any of the peptide sequences in the Antimicrobial Peptide Database (aps.unmc.edu/AP/main.php) (15).

During development of indeterminate nodules, NCR044 and NCR473 transcripts are each highly expressed in the interzone II–III and the nitrogen-fixation zone ZIII and with relatively low expression in the distal and proximal parts of the infection or differentiation zone (FIId and FIIp) (Fig. 1 *C* and *D*) (16). The biological function of each peptide during nodule development and nitrogen fixation remains to be determined. Since NCR044 has been previously demonstrated to inhibit the human fungal pathogen *C. albicans* (8) and is more cationic than NCR473, it was chosen for further studies aimed at determining its structure, antifungal activity against plant fungal pathogens in vitro and in planta, and modes of action as described below.

Expression of Recombinant NCR044 in *Pichia pastoris* and Mass Spectral Analysis of the Purified Peptide. In order to generate the NCR044 peptide with correctly formed disulfide bonds, the NCR044 gene was expressed in a heterologous *Pichia pastoris* expression system. The peptide secreted into the growth medium was successfully purified using cation exchange and C18 reverse-phase high-performance liquid chromatography. Mass spectral analysis revealed a molecular mass of 4311.28 Da for the purified product (*SI Appendix*, Fig. S1 *A* and *B*) as expected for disulfide-linked NCR044. The purity of the NCR044 peptide was determined by sodium dodecyl sulphate-polyacrylamide gel electrophoresis analysis (*SI Appendix*, Fig. S1*C*).

Disulfide Bonding Pattern in NCR044. NCR044 contains four cysteine residues (C9, C15, C25, and C31) with three possible patterns of intramolecular disulfide bond formation and multiple patterns of intermolecular disulfide formation. Since the intra- and intermolecular pattern of disulfide bond formation will significantly affect the peptide's structure, and likely its function, it is important that oxidation is primarily intramolecular and the

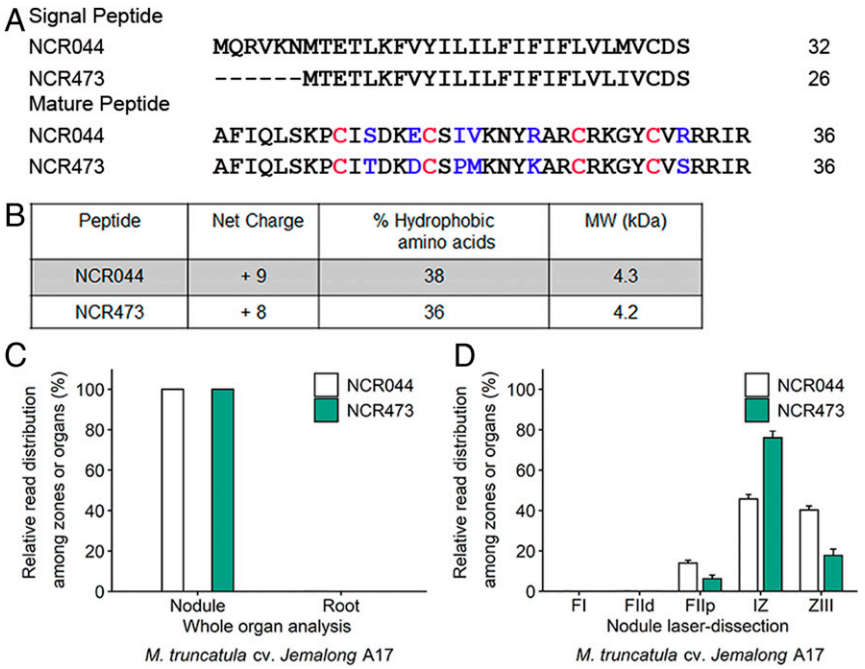

Fig. 1. Amino acid sequences and properties of NCR044 and NCR473 and expression of their genes in root nodules of *M. truncatula* cv. Jemalong A17. (*A*) Primary amino acid sequences of the signal and mature peptide sequences of NCR044 and NCR473. Mature peptide sequences are each 36 residues in length. Conserved cysteine residues are highlighted in red and six nonconserved residues are highlighted in blue. (*B*) Net charge, hydrophobic amino acid content, and molecular weight of the mature NCR044 and NCR473 peptides. (*C*) Gene expression analysis of NCR044 and NCR473 in root nodules and roots at 10 d postinfection (dpi) by *S. meliloti*. (*D*) NCR044 and NCR473 transcript abundance in laser-dissected zones of mature nodules at 15 dpi. FI: nodule meristematic zone, fraction I; FIId: infection zone, distal fraction; FIIp: early differentiation zone, proximal fraction; IZ: late differentiation zone, interzone II–III; ZIII: nitrogen-fixation zone. Web-based RNA sequencing data are available at the Symbimics website (https://iant.toulouse.inra.fr/symbimics).

pattern of oxidation in NCR044 is homogeneous. NMR measurement of the peptide's rotational correlation time (τ_c), 3.6 ± 0.5 ns, was consistent for an ∼4.0-kDa peptide (17), indicating it was primarily monomeric in solution with no detectable intermolecular disulfide bond formation.

Fig. 2 *A* and *B* show the assigned ^{1}H-^{15}N heteronuclear single quantum coherence (HSQC) spectra for the oxidized and reduced forms of NCR044, respectively. For oxidized NCR044 (Fig. 2*A*), the wide chemical shift dispersion of the amide resonances in both the proton and nitrogen dimensions are characteristic features of a structured protein (18). A single set of cross peaks that all could be assigned suggests one dominant species is present with a homogeneous intramolecular disulfide bond pattern. Disulfide bond formation in NCR044 was unambiguously verified from the NMR chemical shifts of the β-carbon of cysteine residues. Generally, the cysteine $^{13}C^{\beta}$ chemical shift in the oxidized state is >35 ppm and decreases to <32 ppm in the reduced state (19). In the absence of Tris(2-carboxyethyl)phosphine (TCEP) or other reducing agents, the cysteine $^{13}C^{\beta}$ chemical shifts for NCR044 were 38.0 ppm or greater, as indicated in *SI Appendix*, Table S1, clearly indicating that cysteine residues were oxidized and incorporated in disulfide bonds. These $^{13}C^{\beta}$ chemical shifts decreased to 28 ppm or less in the presence of 5 mM TCEP, a significant change indicating that disulfide bonds were ablated.

While the chemical shift data indicated disulfide bonds were present, it was not possible to use preliminary structure calculations to deduce unambiguously the disulfide bond pairs from ^{1}H-^{1}H nuclear Overhauser effects (NOEs) due to the consequences of proximal γ-sulfur atoms. Instead, the disulfide bond pattern was deduced from the analysis of mass spectral data for trypsin-digested, unlabeled peptide in the reduced and oxidized states. These data showed that disulfide linkages were C9–C30 and C15–C25. Note that the disulfide bonds are essential for the stability of the peptide's tertiary structure (20) as illustrated in the ^{1}H-^{15}N HSQC spectrum for reduced NCR044 in Fig. 2*B*. The range of chemical shift dispersion of amide resonances was greatly compressed relative to the oxidized NCR044 (Fig. 2*B*), a characteristic feature of disordered proteins (18).

Solution NMR Structure of NCR044. Fig. 2*C* is a superposition of the final ensemble of structures calculated for NCR044 (PDB: 6U6G)

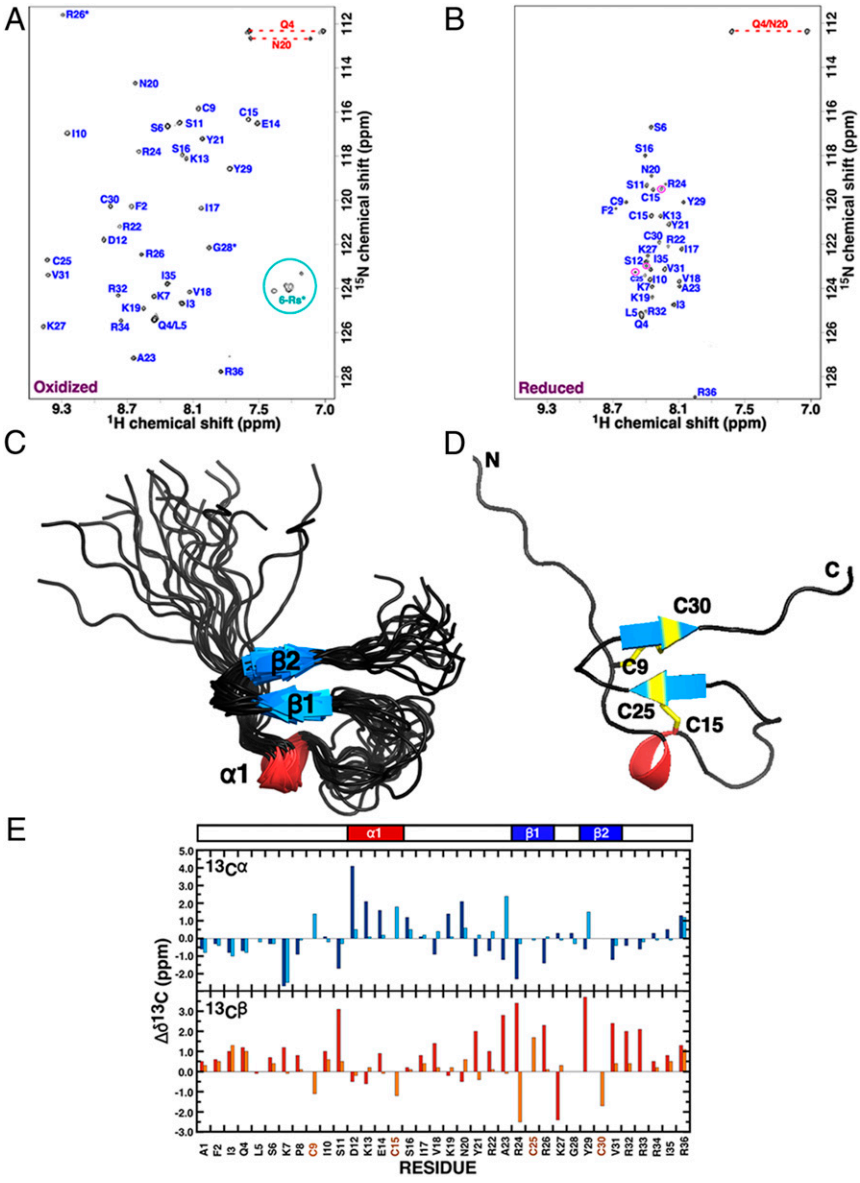

Fig. 2. Solution structure of NCR044. (*A* and *B*) Assigned ^{1}H-^{15}N HSQC spectra for NCR044 (0.7 mM) collected in the (*A*) oxidized (disulfide) and (*B*) reduced (dithiol) states. Spectra collected at 20 °C in 20 mM sodium acetate, 50 mM NaCl, pH 5.3 at a ^{1}H resonance frequency of 600 MHz. Amide side chain resonance pairs are connected by a red dashed line, guanidium protons of the six arginine residues are in the cyan circle (not visible in the reduced state), and folded resonances are identified with an asterisk. The three cross peaks circled in magenta in reduced NCR044 are resonances for R26, R32, or R33 that could not be unambiguously assigned. (*C*) Cartoon representation of the backbone superposition of the ordered regions in the ensemble of 19 structures calculated for oxidized NCR044 (6U6G). β-Strands are colored blue and the α-helix is colored red. (*D*) Cartoon representation of the NCR044 structure closest to the average with a stick representation of the four cysteine side chains highlighted in yellow. (*E*) Analysis of the side chain ^{13}C chemical shifts in the reduced (dithiol) and oxidized (disulfide) states. The observed $^{13}C^{\alpha}$ and $^{13}C^{\beta}$ chemical shift deviations from random coil values for oxidized and reduced NCR044 where $\Delta\delta^{13}C = \delta_{Observed} - \delta_{Random\ coil}$. The random coil carbon values were taken from CNS (cns_solve_1.1) with no calculations for the oxidized cysteine residues. Blue and red, oxidized; cyan and orange, reduced. On top of the graph is a schematic illustration of the elements of secondary structure observed in the NMR-derived structure with the α-helix colored red and β-strands colored blue.

with a single cartoon representation of this ensemble shown in Fig. 2*D*. The most striking feature is the paucity of canonical elements of secondary structure in the peptide. NCR044 contains one short (A23 to R25, G28 to C30) antiparallel β-sheet and a "whiff" (S11 to E14) of an α-helix. The rest of the peptide was largely disordered and dynamic, even with the tethering afforded by the two disulfide bonds. A search for structures in the PDB similar to NCR044 with the DALI server (21) generated no hits, suggesting this structure was new to the PDB. The disorder in the structure was reflected in the paucity of ^{1}H-^{1}H NOEs observed in the nuclear Overhauser effect spectroscopy NMR data. As shown in *SI Appendix*, Table S2, most of the NOEs were intraresidue with only 12 long-range NOEs observed. The prevalent disorder was also reflected in the analysis of the $^{13}C^{\alpha}$ and $^{13}C^{\beta}$ chemical shifts. Deviations of $^{13}C^{\alpha}$ and $^{13}C^{\beta}$ chemical shifts from random coil values are predictive of canonical α-helical (positive $\Delta\delta^{13}C^{\alpha}$, negative $\Delta\delta^{13}C^{\beta}$) and β-strand (negative $\Delta\delta^{13\alpha}$, positive $\Delta\delta^{13}C^{\beta}$) secondary structure (20, 22). These deviations from random coil values were plotted for oxidized and reduced NCR044 in Fig. 2*E* and showed modest correlation for their respective short elements of the secondary structure identified in the NMR structure calculations for the oxidized peptide. Upon reducing the disulfide bonds in the presence of 5 mM TCEP, aside from the N-terminal region (A1 to I10) which was largely disordered in the oxidized state to begin with, these modest correlations disappear with most of the chemical shift values not significantly differing from random coils values. These observations suggest the disulfide bonds play a significant role in stabilizing the structure of the oxidized peptide and in their absence the peptide was largely disordered with little transient structure.

NCR044 Exhibits Potent Antifungal Activity Against Plant Fungal Pathogens. Chemically synthesized NCR044 was previously reported to exhibit fungicidal activity against the human fungal pathogen *C. albicans* at low micromolar concentrations (8). Here, we determined the antifungal activity for recombinant NCR044 against a panel of closely related plant fungal pathogens, *Fusarium* spp. and *B. cinerea*, using a spectrophotometric assay. NCR044 inhibited the growth of *B. cinerea* at low micromolar concentration with a half-maximal inhibitory concentration (IC_{50}) value of 1.55 ± 0.21 μM (Fig. 3*A*). NCR044 also inhibited the growth of *Fusarium graminearum* and *Fusarium virguliforme* with IC_{50} values of 1.93 ± 0.23 and 1.68 ± 0.20 μM, respectively. *Fusarium oxysporum* was most sensitive to NCR044 with an IC_{50} value of 0.52 ± 0.01 μM (Fig. 3*A*). The resazurin cell viability assay revealed that *F. oxysporum* spores lose their cellular metabolic activity at a concentration of 1.5 μM, whereas other fungi, including *B. cinerea*, lose their metabolic activity at a concentration of 3 μM (Fig. 3 *B* and *C*). We also determined the antifungal activity of the chemically synthesized reduced form of the NCR044 peptide against *B. cinerea*. The reduced form of the NCR044 peptide inhibited the growth of *B. cinerea* with IC_{50} value of 4.16 ± 0.18 μM as compared with 1.55 ± 0.21 μM for the native oxidized form of the peptide. The resazurin cell viability assay revealed that *B. cinerea* spores lose their cellular metabolic activity at a concentration of 6 μM as compared with 3 μM for the native oxidized form of the peptide (*SI Appendix*, Fig. S2 *A* and *B*).

NCR044 Disrupts the Plasma Membrane of *B. cinerea*. Antifungal peptides are known to interact with phospholipid bilayers and disrupt the plasma membrane (14). We postulated that the antifungal activity of NCR044 occurred via membrane permeabilization. Using a fluorescent SYTOX Green (SG) nucleic acid staining dye that permeates fungal cells when their plasma membrane integrity is compromised, we tested the ability of NCR044 to permeabilize the plasma membrane of *B. cinerea*.

The uptake of SG in *B. cinerea* spores and germlings treated with 3 μM NCR044 for 15 min was first monitored using confocal microscopy. The nuclei of both spores and germlings were stained with SG, suggesting altered cellular membrane integrity induced by NCR044 (Fig. 4 *A*–*H*). The kinetics of membrane permeabilization was determined in *B. cinerea* germlings treated with various concentrations of NCR044 every 30 min for up to 3 h. In NCR044-treated fungal germlings, permeabilization of the plasma membrane was observed within 30 min and reached its maximal level at 120 min. The rate of membrane permeabilization increased with increasing concentrations of NCR044 as shown in Fig. 4*I*. To test if membrane disruption was sufficient for antifungal activity of NCR044 in ungerminated *B. cinerea* spores, we incubated the spores in 3 μM NCR044 for 1 h, washed off the free peptide, and then allowed the spores to germinate for 24 h at room temperature in peptide-free growth medium. Our data showed that *B. cinerea* spores were able to resume their growth (Fig. 4 *J*–*L*) in a peptide-free growth medium suggesting that, while increased membrane permeability is insufficient to induce death, the peptide served as a potent inhibitor of germination.

NCR044 Elicits Rapid Production of Reactive Oxygen Species (ROS) in *B. cinerea* Germlings, but Much Reduced ROS in Spores of *B. cinerea*. Antimicrobial peptides with a different mode of action are

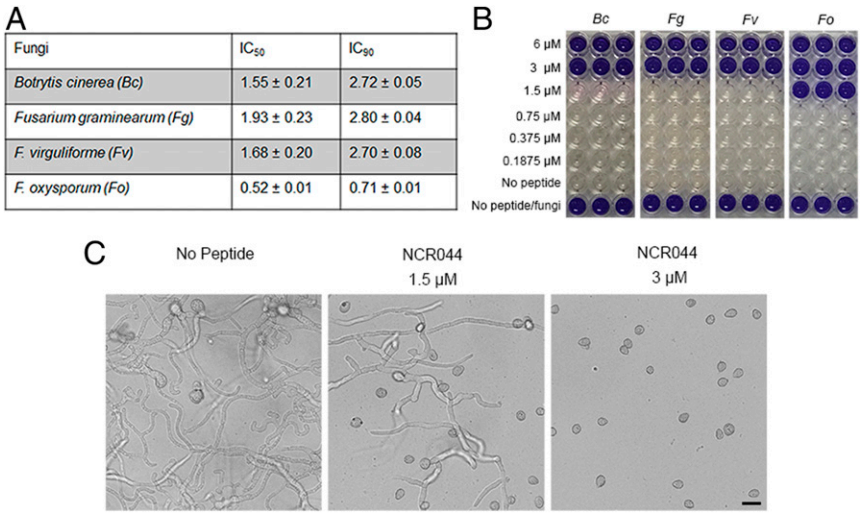

Fig. 3. Antifungal activity of NCR044 against *B. cinerea* and *Fusarium* spp. (*A*) IC_{50} and IC_{90} values of NCR044 for each pathogen are shown. Data are means ± SEM of three independent biological replicates ($n = 3$). (*B*) Results of the fungal cell viability assay using resazurin, a metabolic indicator of living cells. A change from blue to pink/colorless signals resazurin reduction and indicates metabolically active fungal spores after 60 h. In the presence of 3 or 6 μM NCR044, fungal cells lost their metabolic capacity and did not reduce resazurin. (*C*) Representative microscopic images showing the inhibition of *B. cinerea* growth 24 to 48 h after treatment with 1.5 or 3 μM of NCR044 (*Right*). *B. cinerea* without peptide added served as a negative control (*Left*). (Scale bar, 20 μm.)

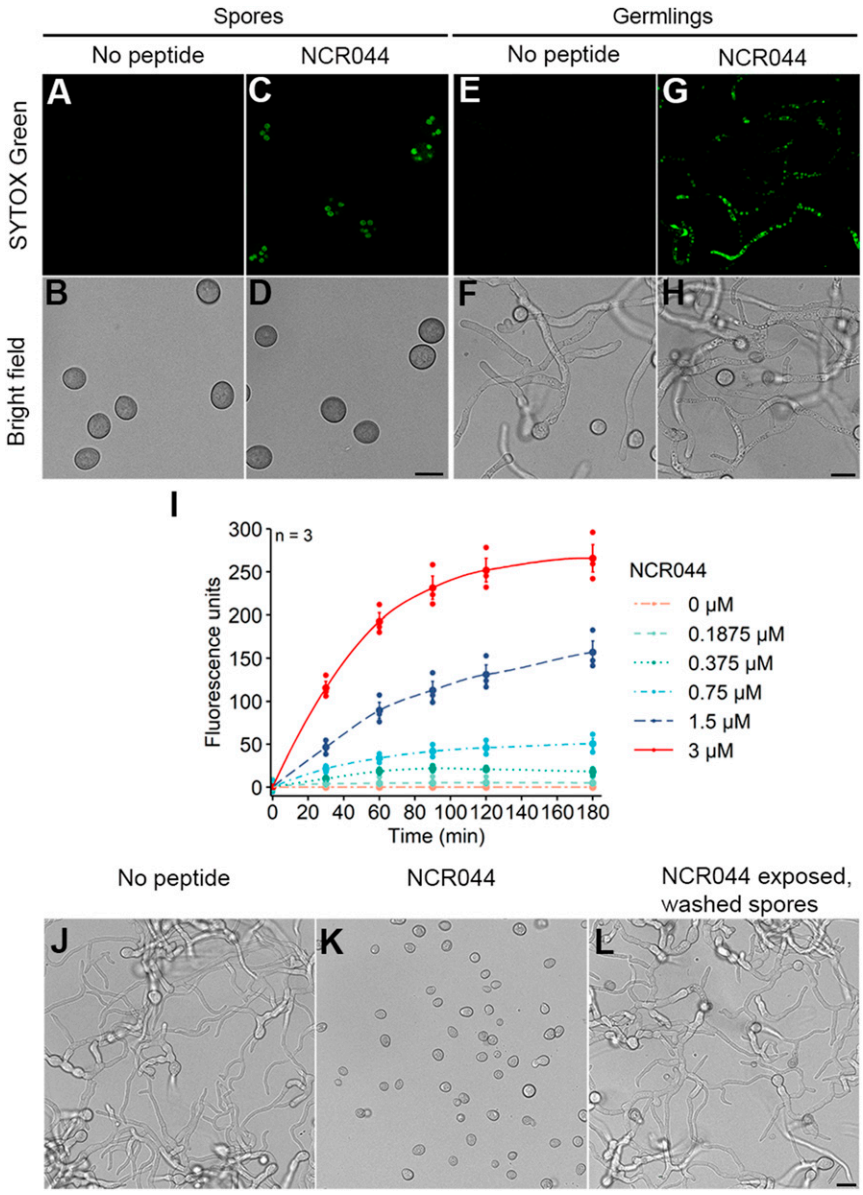

Fig. 4. Membrane permeabilization activity of NCR044. (*A–H*) Confocal microscopy images and corresponding bright field images of SYTOX Green (SG) uptake in *B. cinerea* spores and germlings treated with 3 μM NCR044 for 15 min. (Scale bar, 10 μm.) SG (green) labeled nuclei in spores and germlings treated with NCR044 indicate increased plasma membrane permeability. (*I*) Real-time quantification of cell membrane permeability in *B. cinerea* germlings treated with various concentrations of NCR044. Membrane permeabilization increased with increasing concentrations of peptide. Data are means (large dots) ± SEM of three biological replicates (n = 3, small dots). (*J*) Representative microscopic images of *B. cinerea* spore germination without peptide (*Left*). (*K*) *B. cinerea* growth inhibition in the presence of 3 μM NCR044 (*Middle*). (*L*) The germination of *B. cinerea* spores 24 h after removal of 3 μM NCR044 after treatment with peptide for 1 h (*Right*). (Scale bar, 20 μm.) Fungal growth after removal of the peptide indicates that membrane permeabilization is insufficient for fungal cell death, but germination was inhibited by its presence in media.

known to induce ROS and cause cell death putatively through apoptosis or necrosis-like processes (23, 24). To determine if NCR044 elicited production of ROS, we challenged the spores and germlings of *B. cinerea* with 3 μM of NCR044 for 2 h in the presence of the dye 2′,7′-dichlorodihydrofluorescein diacetate (H_2DCFDA). Upon intracellular oxidation by ROS, H_2DCFDA is converted into a highly fluorescent 2′,7′-dichlorofluorescein (DCF) that can be monitored using confocal microscopy. ROS production was observed in germlings, but not in spores (*SI Appendix*, Fig. S3 *A–F* and *M–R*). Indeed, relative to germlings, only very weak ROS fluorescence signal was detected in spores even after overnight incubation in peptide and histogram rescaling to enhance the very-low-level ROS signals (*SI Appendix*, Fig. S3 *G–L*). Real-time quantification of ROS production was measured spectrophotometrically every 30 min for up to 2 h with untreated germlings and germlings treated with 3 μM NCR044. Rapid induction of ROS fluorescence within 30 min was observed and the fluorescence intensity increased in a time- and dose-dependent manner. The highest fluorescence intensity was observed at 3 μM, suggesting the elicitation of oxidative stress by ROS in germlings following NCR044 treatment (*SI Appendix*, Fig. S3*S*).

NCR044 Binds to Multiple Membrane Phospholipids. Several antifungal defensins have been shown to recruit plasma membrane-resident phospholipids as part of their MOA (24–26). Using the protein–lipid overlay assay, we assessed the ability of NCR044 to bind different bioactive membrane phospholipids. NCR044 strongly bound to phosphatidylinositol 3,5-bisphosphate [PI(3,5)P_2]. It also bound weakly to multiple other phosphoinositides and to phosphatidic acid (PA) (Fig. 5 *A* and *B*). To further investigate the phospholipid-binding specificity of NCR044, a polyPIPosome assay was performed with polymerized liposomes. As shown in Fig. 5*C*, NCR044 bound strongly to liposomes that contained PC:PE:PI(4)P and PC:PE:PI(3,5)P_2 and weakly to PC:PE containing liposomes.

NMR Spectroscopy Reveals Interaction of NCR044 with PI3P. On the basis of the above protein–phospholipid overlay assay, we conducted an NMR chemical shift perturbation study with

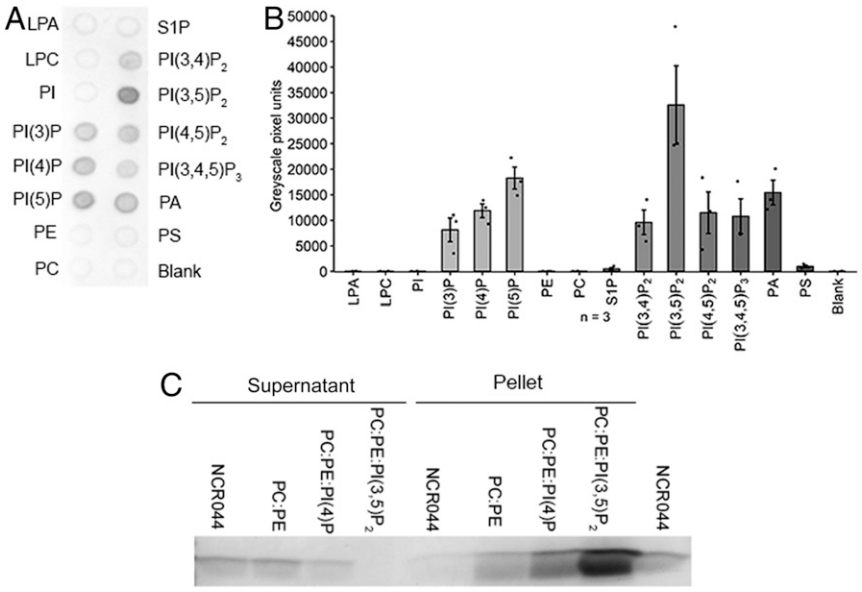

Fig. 5. Phospholipid binding of NCR044. (*A*) PIP strip showing strong binding of NCR044 to phosphatidylinositol diphosphate PI(3,5)P_2 and weak binding to multiple phospholipids, including phosphatidylinositol monophosphates PI(3)P, PI(4)P, and PI(5)P, phosphatidylinositol di/triphosphates PI(3,4)P_2, PI(4,5)P_2, PI(3,4,5)P_3, and phosphatidic acid (PA). (*B*) Densitometry analysis of PIP strip probed with NCR044. Data are means ± SEM of three independent biological replicates (n = 3, small dots). (*C*) PolyPIPosome binding assay showing strong binding of NCR044 to PI(4)P and PI(3,5)P_2 and weak binding to PC:PE.

^{15}N-labeled oxidized NCR044 and PI(3)P to further corroborate phospholipid binding, and ideally, identify the lipid binding surface of NCR044. This experiment is based on the premise that backbone amide protons are sensitive to their molecular environment, and consequently, it is possible to identify the surface of ligand binding to a polypeptide by following amide chemical shift (or intensity) perturbations in ^{1}H-^{15}N HSQC spectra following the titration of ligand into the sample (27, 28). For NCR044, no chemical shift perturbations were observed over the titration range, but the intensity of the amide cross peaks was observed to decrease starting at a PI(3)P:NCR044 molar ratio of 9.4:1. As shown in *SI Appendix*, Fig. S4*A*, there were remnants of only 12 amide cross peaks at a PI(3)P:NCR044 molar ratio of 18.8:1. These intensity perturbations in the ^{1}H-^{15}N HSQC spectra of NCR044 showed that the peptide was interacting with PI(3)P (29). This was corroborated by overall rotational correlation time (τ_c) measurements of the peptide at each titration point that increased from 3.6 ± 0.5 ns in the absence of PI(3)P to 8.7 ± 2.5 ns at a PI(3)P:NCR044 molar ratio of 18.8:1. The latter τ_c value corresponded to a molecular weight in the 15-kDa range (17). Because amide cross peaks should be readily detectable in the ^{1}H-^{15}N HSQC spectrum of an ∼15-kDa species, potential explanations for the disappearing amide resonances include 1) heterogeneous binding to the phospholipid that generates multiple different chemical environments for the peptide with populations that cannot be detected and 2) dynamic interactions with a large molecular complex formed by PI(3)P in solution. To the best of our knowledge, the solution properties of PI(3)P have not been characterized at high concentrations. However, given the aliphatic tails on one end of the molecule and the hydrophilic inositol head group on the other end, it is possible that PI(3)P forms high molecular weight micellar structures at high lipid concentrations. Interactions between PI(3)P and NCR044 are likely electrostatic in nature. The hydrophilic head group of PI(3)P contains two negatively charged phosphate groups. As shown in *SI Appendix*, Fig. S4*B*, the surface of NCR044 is dominated by a positively charged surface that covers the majority of the peptide, providing multiple sites for binding to the hydrophilic head group of PI(3)P.

Exogenous NCR044 Is Translocated into the Cells of *B. cinerea*. We used DyLight550-labeled NCR044 to examine its intracellular translocation into the *B. cinerea* spores and germlings. In spores incubated with 3 μM DyLight550-NCR044, the peptide first accumulated on the cell surface within 1 h (*SI Appendix*, Fig. S5 *A–F*), while only 7.7 ± 2.2% of spores internalized peptide. However, *B. cinerea* spores increased peptide uptake following overnight incubation with diffuse localization in the cytoplasm. Specifically, we quantified the percentage of spores that internalized DyLight550-labeled NCR044 following overnight incubation and observed a significant increase (P = 0.0057, t = −5.4, degrees of freedom [df] = 4, unpaired Student's t test) (Fig. 6 *A–C*) with internalization in 18.8 ± 2.2% in 1.5 μM and 47.5 ± 4.8% in 3-μM treated spores. We also treated spores overnight with 3 μM DyLight550-labeled NCR044, washed off the unbound peptide, and then allowed the spores to germinate in peptide-free growth medium. Our data showed that *B. cinerea* spores were able to resume their growth (*SI Appendix*, Fig. S6 *A–F*) and broad spore death had not occurred, suggesting that the continuous presence of peptide in solution was required to block germination. The continuous presence of DyLight550-labeled NCR044 blocked germination of *B. cinerea* spores (*SI Appendix*, Fig. S6 *G–L*). The membrane selective dye FM4-64 was subsequently used to determine if DyLight550-labeled NCR044 colocalized with cellular membranes in *B. cinerea* germlings. In spore heads and germlings, NCR044 first bound to the cell wall (Fig. 6 *D–F*, arrows) and cell membrane (Fig. 6 *D–F*, arrowheads). NCR044 colocalized with FM4-64 at bright foci at the germling tip and small foci intermittently along the cell periphery of *B. cinerea* (Fig. 6 *G–I*, asterisks). This suggested that this peptide likely interacted with plasma membrane resident phospholipids which invaginated and/or endocytosed to enter fungal cells. Additionally, we observed that NCR044 was distributed diffusely in the cytoplasm and concentrated within the nucleus (Fig. 6 *D–I* and *N*), whereas FM4-64 showed clear cytoplasmic membrane profiles and was excluded from the nucleus, suggesting that NCR044 localized at other nonmembrane intracellular structures.

Next, we applied time-lapse confocal microscopy to monitor the uptake of 3 μM DyLight550-labeled NCR044 in germlings. The peptide initially was observed associated with the germling cell wall (Fig. 6*J*, T = 0 and 3:55, arrowheads) and then migrated toward foci at the germling tip (Fig. 6*J*, T = 0, asterisks) or the germling and/or spore cell walls (Fig. 6*J*, T = 0 through T = 9:51, asterisks). These foci appeared to be the sites of cytoplasmic entry and coincided with a gradual loss of turgor (compare Fig. 6*J* T = 0 with T = 36:41). Within 15 min, the peptide, in

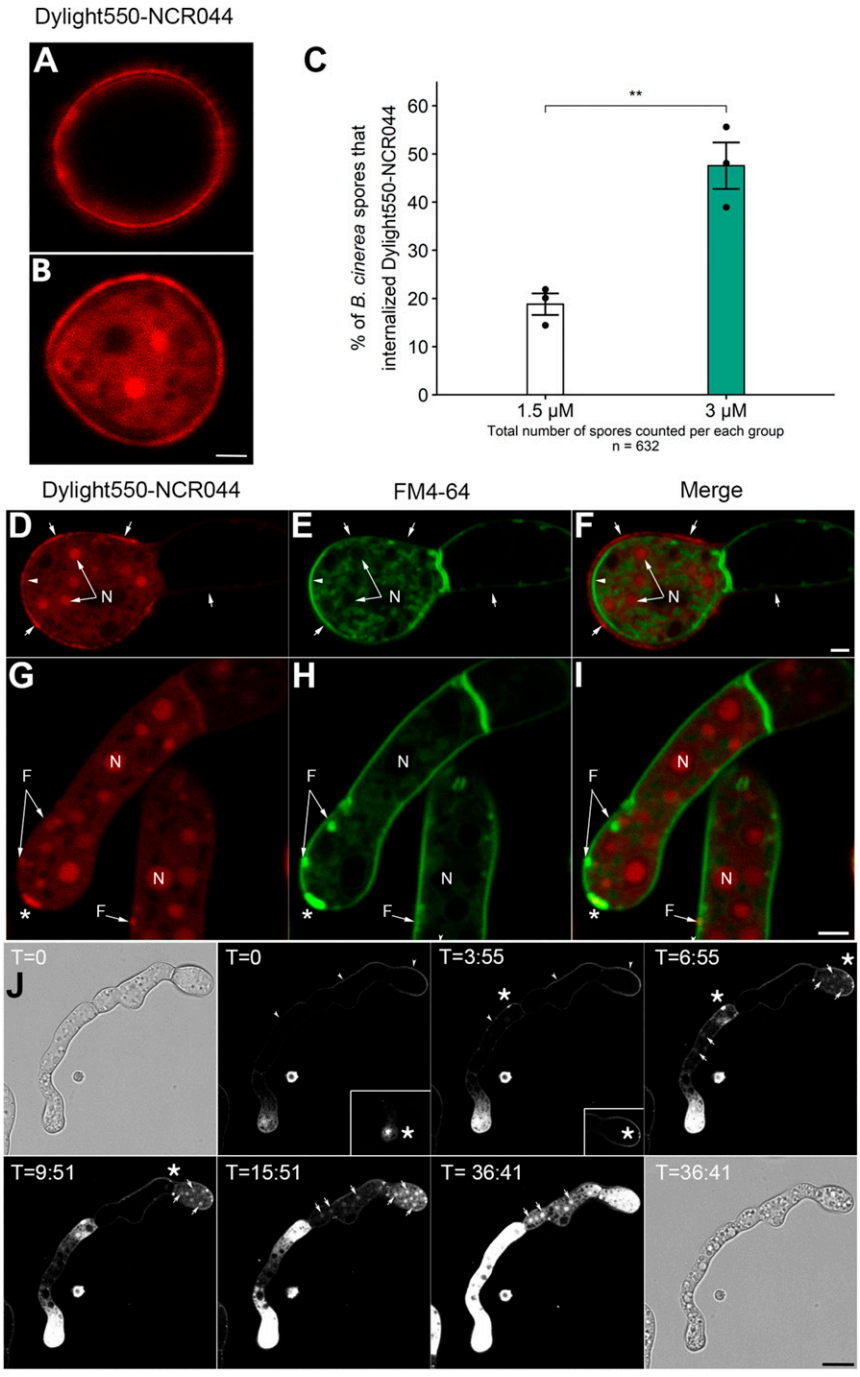

Fig. 6. Translocation of exogenous NCR044 into *B. cinerea* cells. (*A* and *B*) Confocal microscopy images of *B. cinerea* spores showing the uptake of DyLight550-NCR044. NCR044 first accumulated on the cell surface and was internalized inside the *B. cinerea* spores after overnight incubation. (Scale bar, 2 μm.) (*C*) Percentage of *B. cinerea* spores that internalized DyLight550-NCR044 following overnight incubation with 1.5- and 3-μM labeled peptide. Data are means ± SEM of three independent biological replicates ($n = 3$, small dots). Asterisks denote significant differences (**$P < 0.01$, unpaired Student's *t* test). (*D–I*) Confocal microscopy images of *B. cinerea* spore heads and germlings showed the internalization and colocalization of 3 μM Dylight550-NCR044 (red) with membrane-selective dye FM4-64 (green). DyLight550-NCR044 bound to the cell wall (arrows) and cell membranes (arrowheads). DyLight550-NCR044 colocalized with FM4-64 and bright focal accumulations at the germling tip (asterisks) and intermittently adjacent to cell walls (*F*) of *B. cinerea*. DyLight550-NCR044 localization to nuclear region (N). (Scale bar, 2 μm.) (*J*) Time-lapse confocal microscopy images of *B. cinerea* germlings showed internalization of Dylight550-NCR044 (white) over ∼40 min. Peptide first accumulated along cell wall (T = 0) and then entered inside the *B. cinerea* at foci (asterisks) at the germling tip or along the germling and/or spore cell walls (T = 0 through T = 9:51 min). Peptide was diffusely localized into the cytoplasm and a strong signal was observed throughout the nuclear region of spore heads and germlings (T = 9:51 through 36:41 min, arrows). Bright field images at T = 0 and T = 36:41 show loss of turgor and cytoplasmic vacuolization. (Scale bar, 10 μm.)

general, was diffusely localized in the cytoplasm of the germlings and tended to associate with bright spherical structures consistent with nuclei (Fig. 6*J*, T = 6:55 through 36:41, arrows). Often, early entry into the cytoplasm was observed as a gradient across the cell dependent on the origin of plasma membrane breach.

Superresolution Microscopy Reveals Nucleolar Localization of NCR044 in *B. cinerea*. We applied lattice structured illumination microscopy to clearly identify the subcellular localization of DyLight550-labeled NCR044 *in B. cinerea* at high resolution. Since we determined that DyLight550-labeled NCR044 was preferentially localized to the nucleus of *B. cinerea* (Fig. 7 *A* and *B*), we applied the DNA staining dye DAPI to see if the peptide bound to the nuclear DNA. As shown in Fig. 7*C*, DyLight550-NCR044 did not colocalize with DAPI in the nuclei of the germlings, and indeed, appeared to be explicitly excluded from nuclear DNA. We then used the nucleolus-specific RNA staining dye, Nucleolus Bright Green (NBG), to monitor the colocalization with the peptide. We observed that DyLight550-NCR044 strongly colocalized with NBG (Fig. 7*D*) at the site of ribosomal biogenesis.

Fluorescence Recovery after Photobleaching Experiments Reveal that NCR044 Has Strong Binding Affinity to *B. cinerea* Spore Cell Walls and Increased Affinity to the Nucleolus in Germlings. In order to understand the mobility of DyLight550-NCR044 to specific subcellular domains in *B. cinerea*, we performed a series of fluorescence recovery after photobleaching (FRAP) experiments

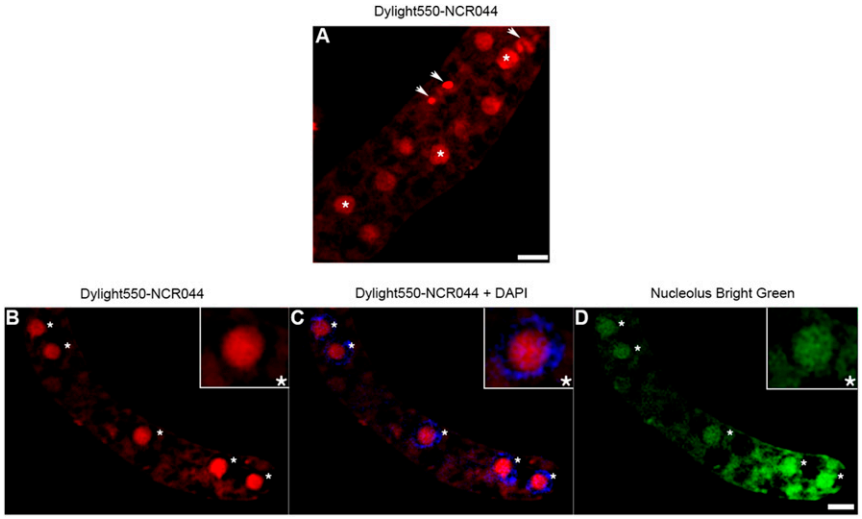

Fig. 7. Subcellular localization of fluorescently labeled DyLight550-NCR044 in *B. cinerea* germlings. (*A*) Superresolution structured illumination microscopy (SR-SIM) images of *B. cinerea* germlings showed the internalization of DyLight550-NCR044 (red). DyLight550-NCR044 was localized at elevated levels to the nucleus in *B. cinerea* germlings (asterisks). (*B*) DyLight550-NCR044 (*C*) did not colocalize with the DNA-specific DAPI (asterisks) stain (*D*), but, colocalized with rRNA specific Nucleolus Bright Green stain showing that NCR044 localized at the nucleolus. Images were taken after 1 h of exposure to 3 μM DyLight550-NCR044. (Scale bar, 2 μm.)

(*SI Appendix*, Fig. S7 *A–E*) quantifying the half time of recovery ($\tau_{1/2}$) of the mobile fraction and percent immobile fraction. We targeted four distinct regions: spore cell wall, germling cell wall, germling cytoplasm, and germling nucleoli, using identical FRAP bleach/recovery acquisition and analysis conditions. Statistically significant differences ($K–W_{statistic} = 59.79$, df = 3, $P < 0.0001$) were observed between specific cellular structures and among the immobile fractions of spore cell wall versus germling cell wall, germling cytoplasm, and germling nucleoli (pairwise Wilcoxon test, corrected $P < 0.0001$) (*SI Appendix*, Fig. S7*B*). Our data showed that the fungal spore cell walls had the highest affinity to DyLight550-NCR044 with an immobile fraction of 76.7 ± 1.3% (spore cell wall) and 24.9 ± 3.2% (germling cell wall), while the germling nucleoli and germling cytoplasm had greatly reduced immobile fractions of 15.4 ± 1.9% and 11.7 ± 1.5%, respectively (*SI Appendix*, Fig. S7*C*). Additionally, the $\tau_{1/2}$ of the mobile fractions revealed a statistically significant difference ($K–W_{statistic} = 27.81$, df = 3, $P < 0.0001$), between germling nucleoli versus germling cytoplasm (pairwise Wilcoxon test, corrected $P < 0.01$) and germling nucleoli versus germling cell wall (corrected $P < 0.01$) (*SI Appendix*, Fig. S7*D*). The spore cell walls and germling nucleoli had the slowest mobility with a $\tau_{1/2}$ = 36.0 ± 2.4 and 31.4 ± 2.4 s, respectively, while the germling cytoplasm and germling cell wall had the fastest mobility with a $\tau_{1/2}$ = 22.0 ± 1.7 and 20.5 ± 3.4 s, respectively (*SI Appendix*, Fig. S7*E*). Taken together, these data suggested that strong binding of the spore cell wall by NCR044 might serve to inhibit germination and/or anchor it in close proximity to the plasma membrane and then upon germination, the mobility of NCR044 increased, allowing it to breach the cell membrane and migrate to cytoplasmic targets.

NCR044 Confers Resistance to *B. cinerea* in Lettuce Leaves and Rose Petals. NCR044 was tested for its ability to reduce symptoms of gray mold disease in planta. Detached lettuce leaves were drop inoculated with the spores of *B. cinerea* in the presence of different concentrations of the peptide. Significant differences in disease severity were found between leaves treated with peptide and control leaves without peptide treatment ($K–W_{statistic}$ = 31.15, df = 3, $P < 0.0001$). In particular, lettuce leaves inoculated with the pathogen in the presence of 6 and 12 μM NCR044 displayed significantly smaller lesions 48 h postinoculation compared to control leaves inoculated with pathogen only (pairwise Wilcoxon test, corrected $P < 0.0001$) (*SI Appendix*, Fig. S8 *A* and *B*).

NCR044 was also tested for its ability to confer resistance to *B. cinerea* in a rose petal infection assay. It significantly reduced virulence of the pathogen on rose petals as compared with control petals without peptide treatment ($K–W_{statistic} = 76.36$, df = 3, $P < 0.0001$). Almost complete suppression of disease symptoms was observed at a concentration of 1.5 μM peptide compared to rose petals inoculated with pathogen only (pairwise Wilcoxon test, corrected $P < 0.0001$) (*SI Appendix*, Fig. S8 *C* and *D*).

Spray-Applied NCR044 Confers Gray Mold Resistance in *N. benthamiana* and Tomato Plants and Is Not Internalized by Plant Cells. We tested the potential of NCR044 for use as an antifungal peptide for controlling gray mold disease in young *N. benthamiana* and tomato plants. At a concentration of 24 μM, NCR044 was sprayed onto the leaves of 4-wk-old *N. benthamiana* and 15-d-old tomato plants and allowed to dry. The Kruskal–Wallis test showed significant differences in disease severity between different treatment groups of *N. benthamiana* ($K–W_{statistic} = 22.75$, df = 2, $P < 0.0001$) and tomato plants ($K–W_{statistic} = 29.06$, df = 2, $P < 0.0001$). *N. benthamiana* and tomato plants sprayed with the peptide had significantly reduced disease symptoms at 48 h (pairwise Wilcoxon test, corrected $P < 0.01$, Fig. 8 *A* and *B*) and 60 h (pairwise Wilcoxon test, corrected $P < 0.01$, Fig. 8 *C* and *D*) postinoculation, respectively, compared to control plants sprayed with pathogen only. The photosynthetic efficiency (variable fluorescence over saturation level of fluorescence [Fv/Fm]) of the control plants (no peptide) exposed to pathogen was significantly lower compared to plants sprayed with NCR044 prior to pathogen exposure. In an effort to determine if defensin internalization/localization observed in fungi also occurred with plant cells, we applied a droplet of 24 μM DyLight550-NCR044 to the leaf surface of *N. benthamiana* and imaged it by confocal microscopy. Our results indicated that DyLight550-NCR044 remained on the plant surface, concentrating at anticlinal walls, with no evidence of internalization within the leaf epidermal cells (*SI Appendix*, Fig. S9 *A–I*).

Discussion

M. truncatula expresses ~700 NCR peptides during the establishment of successful symbiosis with *S. meliloti* (2–4). These peptides are thought to be involved primarily in causing differentiation of the rhizobacteria into bacteroides. However, a subset of these peptides with high cationicity exhibit antimicrobial activity in vitro and in planta (30). Several NCR peptides have now been shown to exhibit bactericidal activity against various

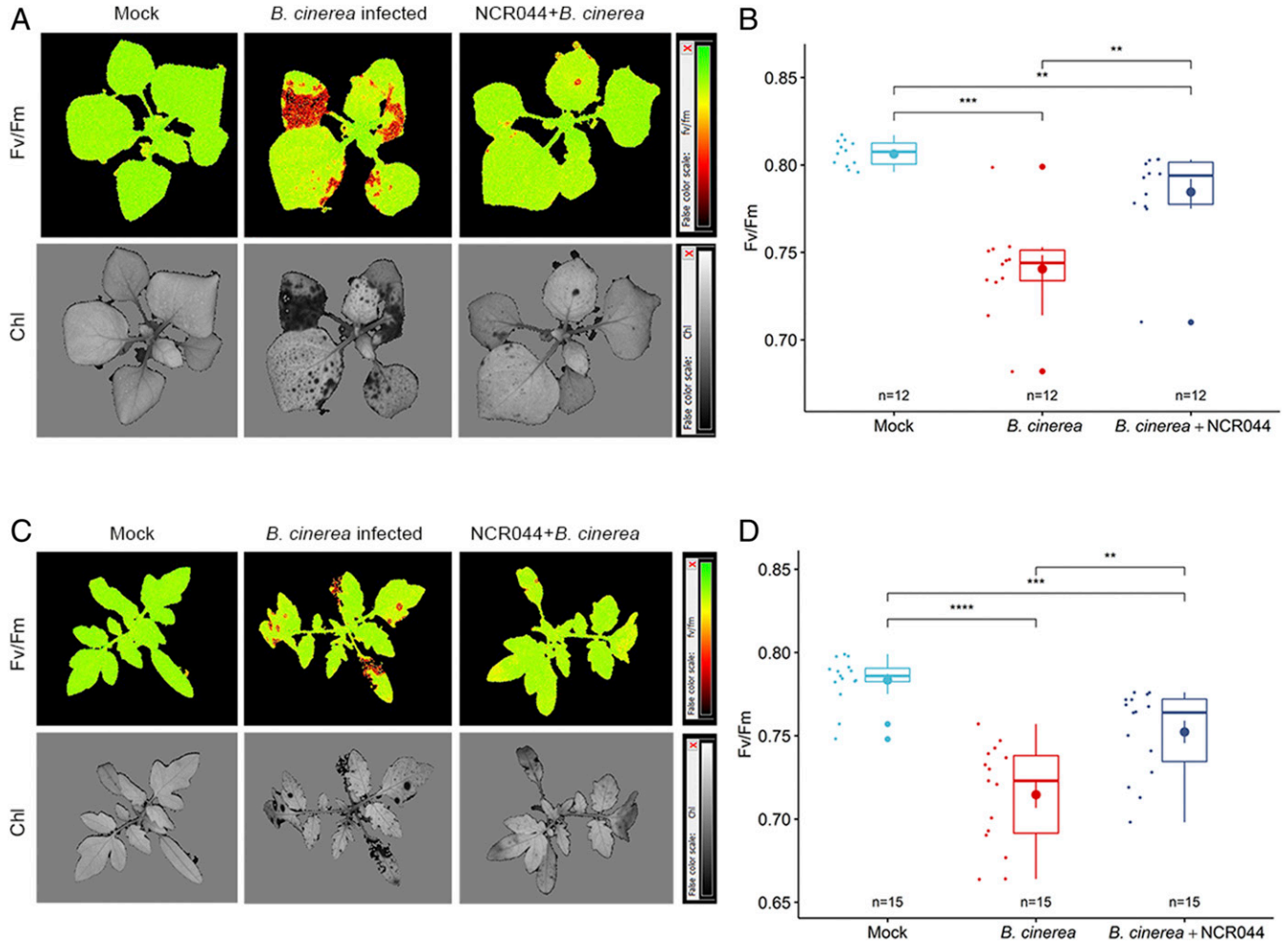

Fig. 8. Spray application of NCR044 confers gray mold resistance in *N. benthamiana* and tomato plants. (*A* and *B*) Four-wk-old *N. benthamiana* and (*C* and *D*) 2-wk-old *Solanum lycopersicum* L. cv. Mountain Spring plants sprayed with either 2 mL water or NCR044 (24 μM) prior to exposure with a spray containing 1 mL of a 5×10^4 *B. cinerea* fungal spore suspension. Maximum quantum yield of PSII photochemistry (Fv/Fm) and the chlorophyll (Chl) index were measured after 48 h (*N. benthamiana*) and 60 h (tomato), after fungal exposure. The false color gradient scale next to the figure indicates the efficiency of photosynthesis. Red (Fv/Fm) or black (Chl) colors represent a low efficiency of photosynthesis, characteristic of stress caused by the interaction between the pathogen and plant. Green (Fv/Fm) or gray (Chl) colors indicate higher efficiency of photosynthesis. NCR044 significantly protected tobacco and tomato plants from gray mold disease caused by *B. cinerea*. The calculated photosynthetic quantum yield (Fv/Fm) of (*B*) tobacco and (*D*) tomato plants. Each colored boxplot represents the 25th and 75th percentiles (box), and the whisker represents 1.5 times the interquartile range (IQR) from the 25th and 75th percentiles. The horizontal line in the box plot represents the median with the mean ± SEM denoted by a dot. Outliers are indicated by large dots outside 1.5*IQR above the first and third quartile. The individual measurements of Fv/Fm are indicated on the *Left* of each boxplot and represent the variances of the samples. The number ($n = 12$) of plants tested is indicated below each group in the boxplot and is from at least two independent experiments for tobacco. Similar results were observed in a third independent experiment, except the data were collected 60 h after fungal exposure. The number ($n = 15$) of plants tested is indicated below each group in the boxplot and is from at least three independent experiments for tomato. Asterisks represent significant differences between different groups (**$P < 0.01$, ***$P < 0.001$, ****$P \leq 0.0001$, pairwise Wilcoxon test with Holm correction, Kruskal–Wallis for multiple groups).

gram-negative and gram-positive bacteria in vitro (3, 10). Among the hundreds of NCR peptides expressed are two NCR044 homolog peptides that share 83% sequence identity and high cationicity. In this study, we report the structure, antifungal activity, and MOA of one of these peptides, NCR044. In addition, we demonstrate its potential for control of pre- and postharvest fungal diseases.

Pre- and postharvest fungal diseases cause substantial losses in the yields of many important crops. These diseases are currently mitigated primarily through application of chemical fungicides multiple times. Unfortunately, such chemical fungicides pose considerable health and environmental risks and become ineffective over time due to the evolution of resistance. Alternative means for control of fungal infections are peptide-based antifungal agents applied topically to plants (31). The oxidized form of the NCR044 peptide exhibits potent broad-spectrum antifungal activity in vitro against four economically important fungal pathogens tested in this study. The antifungal activity of the oxidized form of the NCR044 peptide exhibited potency similar to that of other antifungal peptides (25, 26, 31). However, other factors such as a growth medium used in testing the antimicrobial activities can strongly affect the efficacy of antifungal peptides (32). Our initial experiments with a reduced form of the NCR044 peptide showed over a two-fold decrease in the in vitro antifungal activity against *B. cinerea*, indicating the importance of disulfide bonds for increased potency of the oxidized form of NCR044. For deployment of NCR044 in crop protection, one could envisage further manipulating the cationicity/hydrophobicity of the oxidized or reduced NCR044 through site-directed

mutagenesis and increase its antifungal potency on the surface of plant tissues without causing phytotoxicity.

When applied on the surface of lettuce leaves and rose petals, the oxidized form of the NCR044 peptide significantly reduces gray mold disease lesions caused by *B. cinerea* infection. Moreover, spray application of this peptide controls gray mold disease symptoms in young tomato and *N. benthamiana* plants. These data warrant additional studies to investigate the potential of NCR044 as a spray-on peptide antifungal agent for the control of gray mold disease in vegetables, flowers and other economically important crops. In contrast to chemical fungicides, peptide-based "green chemistry" antifungal agents are sustainable and ideal for protection of the environment and consumer health (31).

In the inverted repeat-lacking clade legumes such as *M. truncatula*, two families of cysteine-rich peptides, namely defensins and defensin-like NCRs, are expressed. These two families have likely evolved in parallel in this legume to play different biological roles. While defensins have evolved for defense against harmful pathogens early in the evolution of land plants, NCRs have evolved relatively recently and act as effectors inducing differentiation of rhizobia into nitrogen-fixing bacteroids (5). Therefore, antifungal activity is a secondary attribute of NCR044. However, the possibility cannot be ruled out that it acts in concert with other NCRs to defend differentiating nodules from harmful fungal and bacterial pathogens in *M. truncatula* (33). Antifungal plant defensins with four disulfide bonds are diverse in their amino acid sequences but, their 3D structures with a highly conserved cysteine-stabilized α/β motif are strikingly similar (34, 35). To our knowledge, no 3D structure of an NCR peptide has been determined to date. The structure of NCR044 reported here is dominated by largely disordered regions. It remains to be determined if this disordered structure adopts an ordered secondary structure in membrane-mimetic solutions and contributes to the biochemical function and/or stability of this peptide. It is interesting to note that the predominant disulfide pattern of the oxidized NCR044 (C1 to C4, C2 to C3) is the same as the C1 to C4, C2 to C3 pattern of the predominant derivative of NCR247 oxidized in vitro (33). Several hundred NCR peptides expressed in the nodules of *M. truncatula* also exhibit significant variation in their amino acid sequences and therefore they too may differ substantially in their structures and antifungal MOA (36).

A common characteristic of antifungal peptides is their ability to permeabilize the plasma membrane of fungal pathogens. In plant defensins, membrane permeabilization is also an important early step in their MOA (34, 35). Recently, the peptides NCR192, NCR247, and NCR335 have been reported to disrupt the plasma membrane of *C. albicans* (8). In the mechanistic studies employing NCR044 here, we determined that NCR044 quickly binds to the cell walls of *B. cinerea* spores and germlings and subsequently breaches the plasma membrane of these cells near the attachment sites. Within 30 min after peptide exposure, SYTOX Green uptake was observed at a dose-dependent rate. Thus, membrane permeabilization is also an early step in fungal cell death induced by NCR044. This was further supported by our observation that as cytoplasmic loading of DyLight550-labeled NCR044 peptide occurred, it coincided with concomitant loss of turgor. However, spores temporarily exposed to NCR044 for a period of 1 h or overnight could subsequently germinate. It was noted that peptide localization in ungerminated spores appeared to be largely restricted to the spore wall with few exceptions, (presumed to be compromised dead spores). Taken together, these data showed that the peptide inhibited germination and additionally, the quiescent spores appeared to lack the physiological activity to allow sufficient membrane permeabilization and induce cell death as observed in germlings.

Since several plant defensins bind to plasma membrane resident bioactive phosphoinositides or related phospholipids to oligomerize and induce membrane permeabilization (26, 35), we tested whether NCR044 also bound to specific phospholipids. Like the plant defensins NaD1 (26) and MtDef5 (24), NCR044 bound to several phospholipids in the phospholipid–protein overlay assay. Of note, it bound more effectively to PI mono/diphosphates, in particular, $PI(3,5)P_2$. Further studies are needed to decipher the mechanism by which membrane permeabilization is induced by NCR044 and to understand the role phospholipid binding plays in peptide-induced membrane permeabilization of fungal pathogens.

Inhibition of mitochondrial respiration leads to the generation of ROS that play an important role in fungal cell death (34, 35). Using the dye H_2DCFDA, ROS generation was readily detected in NCR044-challenged germlings, but under the same conditions, not detected in spores of *B. cinerea*. However, very low levels of ROS were observed in spores after long exposure and histogram rescaling. This observation is consistent with the overall reduced peptide uptake in quiescent spores relative to germlings. This was further supported by our observation that *B. cinerea* spores treated with DyLight550-labeled NCR044 following overnight incubation were able to resume their growth after removing the unbound peptide from the media. However, further studies are needed to unambiguously establish NCR044-induced ROS generation as a cause of cell death. In particular, it will be important to obtain evidence for the induction of the markers of ROS-mediated oxidative damage, such as protein carbonylation and DNA laddering, that lead to cell death.

Internalization of NCR044 into the spores and germlings of *B. cinerea* has been studied in relation to its antifungal activity. While NCR044 internalization by spores was slow and limited, it was internalized rapidly by germlings of this pathogen. Our colocalization experiments with FM4-64, an amphiphilic styryl dye that serves as a marker for endocytosis and vesicle trafficking, provided important clues about NCR044 initial entry into fungal cells. The earliest signs of internalization of DyLight550-labeled NCR044 were often indicated by a single patch near the germling tip (Fig. 6 *G* and *J*, T = 0) and smaller foci just beneath the cell wall (Fig. 6 *G–I*) which colabeled with FM6-64. This pattern was similar to that reported for *M. truncatula* defensin MtDef5 in *Neurospora crassa* (24) and consistent with the apical vesicle accumulation and sites of endocytosis observed with FM4-64 and AM4-64 studies in a number of diverse fungi, including *B. cinerea* (37, 38). Once internalized, the peptide appeared to diffuse through the cytoplasm and NCR044 gradients formed (Fig. 6*J*) that coincided with origins of initial cell surface foci but no longer matched the classical membrane/vesicle-labeled pattern of FM4-64 (Fig. 6 *D–I*). Once cytoplasmic, the peptide localized to nucleoli, the site of ribosomal biogenesis. Interestingly, NCR247 has also been shown previously to interact with ribosomal proteins in the symbiont *S. meliloti* (12). While the exact mechanism for nucleolar binding is unknown, electrostatic maps of ribosomal subunits show large areas of negative potential (39) and this property significantly influences interactions with positively charged proteins (40), and conceivably, NCR044 with a net charge of +9. It will be important to determine if other antifungal NCR peptides from IRLC legumes also target nucleoli in fungal cells. Interaction with ribosomes and inhibition of translation are likely to be a shared mechanism used by some antifungal NCR peptides (12). While it is intriguing to speculate that this could be a possible mechanism used by NCR044, further supporting experiments are required to understand the significance of this observation. However, the possibility remains that these peptides have multiple intracellular targets to induce fungal cell death, a notion recently proposed for a highly effective fungicide strategy using monoalkyl chain lipophilic cations (41).

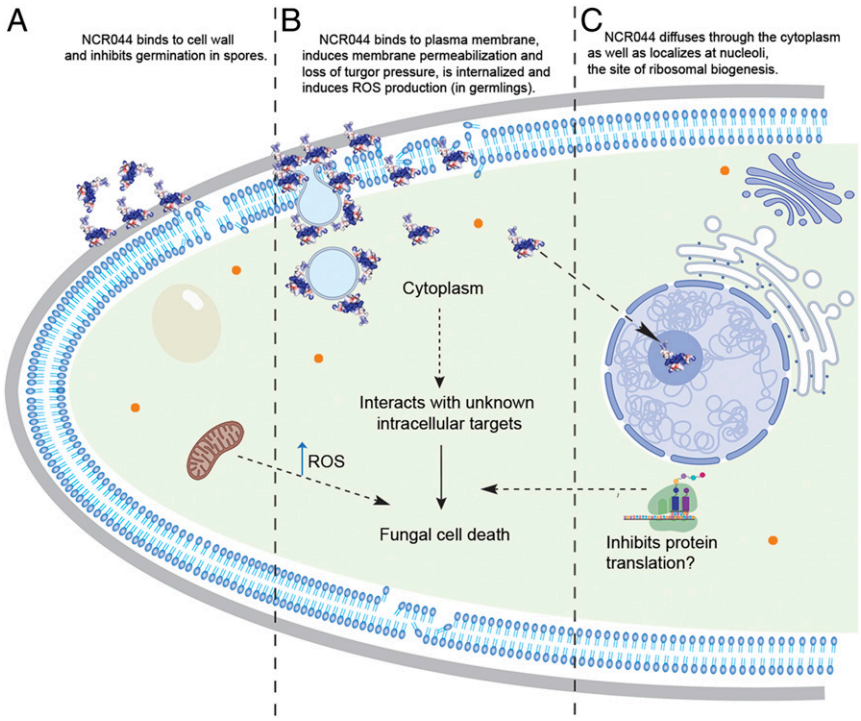

Fig. 9. Proposed multistep model for the antifungal action of NCR044 against *B. cinerea*. (*A*) NCR044 binds to cell wall and inhibits germination in spores. (*B*) NCR044 binds to plasma membrane, induces membrane permeabilization and loss of turgor pressure, is internalized, and induces ROS production (in germlings). (*C*) NCR044 diffuses through the cytoplasm as well as localizes at nucleoli, the site of ribosomal biogenesis.

Based on the results reported here, we propose a multistep model for the antifungal action of NCR044 against *B. cinerea* (Fig. 9 *A*–*C*). The first step involves binding of the peptide to the cell wall and inhibition of germination (when applied to spores) followed by binding and internalization at putative sites of endocytosis and then disruption of the plasma membrane via interaction with membrane-resident phospholipids (in germlings). The peptide eventually gains entry into the cytoplasm, inducing the formation of ROS and localization to nucleoli, where it is hypothesized to interact with ribosomal RNA and/or ribosomal proteins and inhibit protein translation. Our data show that NCR044 interacts with several major and diverse cellular components, perhaps permitted by its highly dynamic structure as determined by NMR, thus allowing broad effectiveness against fungal pathogens. These insights necessitate further studies to better understand the relative contribution of each step to the antifungal action of NCR044. Hundreds of NCR peptides expressed in nodules of certain legumes offer highly diverse antifungal peptide sequence space and this work on NCR044 peptide structure and its MOA will help in the design of more effective antifungal peptides using protein engineering for future use in agriculture.

Materials and Methods

Details of each experimental method, including statistical analysis, fungal cultures, and spore suspensions, recombinant expression and purification of NCR044, ^{15}N and ^{13}C isotopic labeling of NCR044 for NMR structural analysis, NMR spectroscopy of NCR044, NMR solution structure calculations for the oxidized form of NCR044, antifungal activity assay, SG membrane permeabilization assay, quantification of intracellular ROS, NCR044 uptake into fungal cells, FRAP experimental setup and analysis, peptide distribution on the plant surface, NCR peptide–phospholipid interactions, semi-in planta antifungal activity of NCR044 against *B. cinerea*, and evaluation of NCR044 as sprayable peptide for protection against gray mold disease are given in *SI Appendix*.

Data Deposition. The coordinates of the NMR structure have been deposited in the Protein Data Bank, www.rcsb.org (PDB code: 6U6G) and the NMR chemical shifts have been deposited in the BioMagResBank, www.bmrb.wisc.edu (accession no. 30660).

ACKNOWLEDGMENTS. The generous support from TechAccel for part of the research reported here is acknowledged. The structure for NCR044 was solved using resources at the W. R. Wiley Environmental Molecular Sciences Laboratory, a national scientific user facility sponsored by the US Department of Energy's Office of Biological and Environmental Research program located at Pacific Northwest National Laboratory (PNNL). Battelle operates PNNL for the US Department of Energy. We also acknowledge imaging support from the Advanced Bioimaging Laboratory at the Danforth Plant Science Center and usage of the Leica SPX-8 acquired through an NSF Major Research Instrumentation grant (DBI-1337680). We thank Proteomics and Mass Spectrometry Facility at the Danforth Center for conducting mass spectrometry analysis of NCR044.

1. E. Kondorosi, P. Mergaert, A. Kereszt, A paradigm for endosymbiotic life: Cell differentiation of Rhizobium bacteria provoked by host plant factors. *Annu. Rev. Microbiol.* **67**, 611–628 (2013).
2. A. Kereszt, P. Mergaert, J. Montiel, G. Endre, É. Kondorosi, Impact of plant peptides on symbiotic nodule development and functioning. *Front. Plant Sci.* **9**, 1026 (2018).
3. W. Van de Velde *et al*., Plant peptides govern terminal differentiation of bacteria in symbiosis. *Science* **327**, 1122–1126 (2010).
4. J. Montiel *et al*., Morphotype of bacteroids in different legumes correlates with the number and type of symbiotic NCR peptides. *Proc. Natl. Acad. Sci. U.S.A.* **114**, 5041–5046 (2017).
5. G. Maróti, J. A. Downie, É. Kondorosi, Plant cysteine-rich peptides that inhibit pathogen growth and control rhizobial differentiation in legume nodules. *Curr. Opin. Plant Biol.* **26**, 57–63 (2015).
6. B. Horváth *et al*., Loss of the nodule-specific cysteine rich peptide, NCR169, abolishes symbiotic nitrogen fixation in the *Medicago truncatula* dnf7 mutant. *Proc. Natl. Acad. Sci. U.S.A.* **112**, 15232–15237 (2015).
7. M. Kim *et al*., An antimicrobial peptide essential for bacterial survival in the nitrogen-fixing symbiosis. *Proc. Natl. Acad. Sci. U.S.A.* **112**, 15238–15243 (2015).
8. L. Ordögh, A. Vörös, I. Nagy, E. Kondorosi, A. Kereszt, Symbiotic plant peptides eliminate *Candida albicans* both *in vitro* and in an epithelial infection model and inhibit the proliferation of immortalized human cells. *BioMed Res. Int.* **2014**, 320796 (2014).
9. A. Farkas, G. Maróti, A. Kereszt, É. Kondorosi, Comparative analysis of the bacterial membrane disruption effect of two natural plant antimicrobial peptides. *Front. Microbiol.* **8**, 51 (2017).

10. H. Tiricz *et al*., Antimicrobial nodule-specific cysteine-rich peptides induce membrane depolarization-associated changes in the transcriptome of *Sinorhizobium meliloti*. *Appl. Environ. Microbiol.* **79**, 6737–6746 (2013).
11. E. P. Balogh *et al*., Anti-chlamydial effect of plant peptides. *Acta Microbiol. Immunol. Hung.* **61**, 229–239 (2014).
12. A. Farkas *et al*., *Medicago truncatula* symbiotic peptide NCR247 contributes to bacteroid differentiation through multiple mechanisms. *Proc. Natl. Acad. Sci. U.S.A.* **111**, 5183–5188 (2014).
13. B. Alunni, B. Gourion, Terminal bacteroid differentiation in the legume-rhizobium symbiosis: Nodule-specific cysteine-rich peptides and beyond. *New Phytol.* **211**, 411–417 (2016).
14. N. L. van der Weerden, M. R. Bleackley, M. A. Anderson, Properties and mechanisms of action of naturally occurring antifungal peptides. *Cell. Mol. Life Sci.* **70**, 3545–3570 (2013).
15. G. Wang, X. Li, Z. Wang, APD3: The antimicrobial peptide database as a tool for research and education. *Nucleic Acids Res.* **44**, D1087–D1093 (2016).
16. B. Roux *et al*., An integrated analysis of plant and bacterial gene expression in symbiotic root nodules using laser-capture microdissection coupled to RNA sequencing. *Plant J.* **77**, 817–837 (2014).
17. P. Rossi *et al*., A microscale protein NMR sample screening pipeline. *J. Biomol. NMR* **46**, 11–22 (2010).
18. A. Yee *et al*., An NMR approach to structural proteomics. *Proc. Natl. Acad. Sci. U.S.A.* **99**, 1825–1830 (2002).
19. D. Sharma, K. Rajarathnam, 13C NMR chemical shifts can predict disulfide bond formation. *J. Biomol. NMR* **18**, 165–171 (2000).
20. G. W. Buchko *et al*., Cytosolic expression, solution structures, and molecular dynamics simulation of genetically encodable disulfide-rich de novo designed peptides. *Protein Sci.* **27**, 1611–1623 (2018).
21. L. Holm, Benchmarking fold detection by DaliLite v.5. *Bioinformatics* **35**, 5326–5327 (2019).
22. L. Szilágyi, Chemical-shifts in proteins come of age. *Prog. Nucl. Magn. Reson. Spectrosc.* **27**, 325–443 (2002).
23. B. M. E. Hayes *et al*., Identification and mechanism of action of the plant defensin NaD1 as a new member of the antifungal drug arsenal against *Candida albicans*. *Antimicrob. Agents Chemother.* **57**, 3667–3675 (2013).
24. K. T. Islam, S. L. S. Velivelli, R. H. Berg, B. Oakley, D. M. Shah, A novel bi-domain plant defensin MtDef5 with potent broad-spectrum antifungal activity binds to multiple phospholipids and forms oligomers. *Sci. Rep.* **7**, 16157 (2017).
25. M. Järvå *et al*., Human β-defensin 2 kills *Candida albicans* through phosphatidylinositol 4,5-bisphosphate–mediated membrane permeabilization. *Sci. Adv.* **4**, eaat0979 (2018).
26. I. K. Poon *et al*., Phosphoinositide-mediated oligomerization of a defensin induces cell lysis. *eLife* **3**, e01808 (2014).
27. E. R. P. Zuiderweg, Mapping protein-protein interactions in solution by NMR spectroscopy. *Biochemistry* **41**, 1–7 (2002).
28. G. W. Buchko, O. Litvinova, H. Robinson, A. F. Yakunin, M. A. Kennedy, Functional and structural characterization of DR_0079 from *Deinococcus radiodurans*, a novel Nudix hydrolase with a preference for cytosine (deoxy)ribonucleoside 5′-Di- and triphosphates. *Biochemistry* **47**, 6571–6582 (2008).
29. G. W. Daughdrill *et al*., Chemical shift changes provide evidence for overlapping single-stranded DNA- and XPA-binding sites on the 70 kDa subunit of human replication protein A. *Nucleic Acids Res.* **31**, 4176–4183 (2003).
30. P. Mergaert, Role of antimicrobial peptides in controlling symbiotic bacterial populations. *Nat. Prod. Rep.* **35**, 336–356 (2018).
31. P. Schwinges *et al*., A bifunctional dermaseptin–thanatin dipeptide functionalizes the crop surface for sustainable pest management. *Green Chem.* **21**, 2316–2325 (2019).
32. A. Farkas, B. Pap, É. Kondorosi, G. Maróti, Antimicrobial activity of NCR plant peptides strongly depends on the test assays. *Front. Microbiol.* **9**, 2600 (2018).
33. M. Shabab *et al*., Disulfide cross-linking influences symbiotic activities of nodule peptide NCR247. *Proc. Natl. Acad. Sci. U.S.A.* **113**, 10157–10162 (2016).
34. T. L. Cools, C. Struyfs, B. P. Cammue, K. Thevissen, Antifungal plant defensins: Increased insight in their mode of action as a basis for their use to combat fungal infections. *Future Microbiol.* **12**, 441–454 (2017).
35. K. Parisi *et al*., The evolution, function and mechanisms of action for plant defensins. *Semin. Cell Dev. Biol.* **88**, 107–118 (2019).
36. G. Maróti, A. Kereszt, E. Kondorosi, P. Mergaert, Natural roles of antimicrobial peptides in microbes, plants and animals. *Res. Microbiol.* **162**, 363–374 (2011).
37. S. Fischer-Parton *et al*., Confocal microscopy of FM4-64 as a tool for analysing endocytosis and vesicle trafficking in living fungal hyphae. *J. Microsc.* **198**, 246–259 (2000).
38. O. V. Kamzolkina, M. A. Kiselica, O. A. Kudryavtseva, O. V. Shtaer, I. S. Mazheika, Endocytosis and its inhibitors in basidiomycetous fungus *Rhizoctonia solani*. *Moscow Univ. Biol. Sci. Bull.* **72**, 128–136 (2017).
39. N. A. Baker, D. Sept, S. Joseph, M. J. Holst, J. A. McCammon, Electrostatics of nanosystems: Application to microtubules and the ribosome. *Proc. Natl. Acad. Sci. U.S.A.* **98**, 10037–10041 (2001).
40. P. E. Schavemaker, W. M. Śmigiel, B. Poolman, Ribosome surface properties may impose limits on the nature of the cytoplasmic proteome. *eLife* **6**, e30084 (2017).
41. G. Steinberg *et al*., A lipophilic cation protects crops against fungal pathogens by multiple modes of action. *Nat. Commun.* **11**, 1608 (2020).